equivalence should facilitate a more unified approach in understanding all natural enemy-victim interactions. Interpreting spatial heterogeneity in terms of time delays is likely to be a powerful tool for understanding many complex ecological situations. Not only have more statistical tools and more biological intuition been developed to deal with DDD, but in general the data needed to study temporal lags are far more readily attainable than the data needed to study spatial structure.

References and Notes

1. A. J. Lotka, *The Elements of Physical Biology* (Williams & Williams, Baltimore, MD, 1925).
2. V. Volterra, *Nature* **118**, 558 (1926).
3. A. J. Nicholson, V. A. Bailey, *Proc. Zool. Soc. London* **3**, 551 (1935).
4. C. B. Huffaker, *Hilgardia* **27**, 343 (1958).
5. M. P. Hassell, R. M. May, *J. Anim. Ecol.* **43**, 567 (1974).
6. A. Hastings, *Theor. Popul. Biol.* **12**, 37 (1977).
7. R. M. May, *J. Anim. Ecol.* **47**, 833 (1978).
8. I. Hanski, *Ecology* **64**, 493 (1983).
9. P. Kareiva, *Philos. Trans. R. Soc. London Ser. B* **330**, 175 (1990).
10. R. Durrett, S. A. Levin, *Theor. Popul. Biol.* **46**, 363 (1994).
11. M. Keeling, in *Advanced Ecological Theory*, J. McGlade, Ed. (Blackwell Science, Oxford, 1999), pp. 64–99.
12. M. P. Hassell, H. Comins, R. M. May, *Nature* **353**, 255 (1991).
13. E. McCauley, W. G. Wilson, A. M. DeRoos, *Am. Nat.* **142**, 412 (1993).
14. S. W. Pacala *et al.*, *Ecol. Monogr.*, **66**, 1 (1996).
15. E. Renshaw, *Modelling Biological Populations in Space and Time* (Cambridge Univ. Press, Cambridge, 1991).
16. M. Keeling, *J. Anim. Ecol.* **69** 725 (2000).
17. B. M. Bolker, S. W. Pacala, *Am. Nat.* **153**, 575 (1999).
18. The full equations for the numbers of hosts (H) and parasites (or parasitoids) (P) clearly depend on a higher moment, namely the average covariance $\bar{C}_t$. By considering all stochastic events that can occur, we can also formulate an equation describing the dynamics of $\bar{C}_t$; however, this will also include higher moments. The moment closure analysis approximates these higher moments by their equivalent values for a Poisson distribution. When the movement rates are large, the effect of this Poisson assumption on the covariance is small and the corresponding effects on the mean number of H and P is smaller still. Extensive simulations have shown that approximations of this order are still valid even when the movement rates are quite small. The full derivation of the equations and stability analysis is given in the supplementary Web material (*29*).
19. D. S. Broomhead, G. P. King, *Physica D* **20**, 217 (1986).
20. H. B. Wilson, D. A. Rand, *Proc. R. Soc. London Ser. B* **264**, 625 (1997).
21. M. P. Hassell, *The Dynamics of Arthropod Predator-Prey Systems* (Princeton Univ. Press, Princeton, NJ, 1978).
22. S. W. Pacala, M. P. Hassell, *Am. Nat.* **138**, 584 (1991).
23. P. Turchin, *Nature* **344**, 660 (1990).
24. B. Hornfeldt, *Ecology* **75**, 791 (1994).
25. O. N. Bjornstad *et al.*, *J. Anim. Ecol.* **67**, 110 (1998).
26. T. Saitoh, N. C. Stenseth, O. N. Bjornstad, *Res. Popul. Ecol.* **40**, 61 (1998).
27. E. E. Crone, *Theor. Popul. Biol.* **51**, 67 (1997).
28. D. J. Rodriguez, *J. Theor. Biol.* **191**, 95 (1998).
29. Available on *Science* Online at www.sciencemag.org/cgi/content/full/290/5497/1758/DC1

30. We thank M. Hassell for his valuable comments on the manuscript. M.J.K. is supported by a Royal Society University Training Fellowship. H.B.W. is supported by a National Environment Research Council Advanced Fellowship.

16 August 2000; accepted 11 October 2000

Posttranslational N-Myristoylation of BID as a Molecular Switch for Targeting Mitochondria and Apoptosis

Jiping Zha,* Solly Weiler,* Kyoung Joon Oh, Michael C. Wei, Stanley J. Korsmeyer†

Many apoptotic molecules relocate subcellularly in cells undergoing apoptosis. The pro-apoptotic protein BID underwent posttranslational (rather than classic cotranslational) N-myristoylation when cleavage by caspase 8 caused exposure of a glycine residue. N-myristoylation enabled the targeting of a complex of p7 and myristoylated p15 fragments of BID to artificial membranes bearing the lipid composition of mitochondria, as well as to intact mitochondria. This post-proteolytic N-myristoylation serves as an activating switch, enhancing BID-induced release of cytochrome c and cell death.

Localization of proteins to distinct subcellular compartments, including membranes, is a critical event in multiple cellular pathways such as apoptosis. Discrete topogenic sequence elements within proteins function as an address for unidirectional targeting to select membrane sites (*1*). Alternatively, lipid modification of proteins, including isoprenylation, myristoylation, palmitoylation, or modification by glycosyl-phosphatidylinositol, enables targeting and permits stable membrane association (*2*, *3*). One drastic cell fate decision, apoptosis, follows signal transduction events and results in the redistribution of proteins, which often initiates their effector activity. Phosphorylation, a well-documented mechanism that can relocate proteins (*4*), regulates the movement of pro-apoptotic BAD from cytosol to mitochondria (*5*) and the movement of Forkhead transcription factor (FKHRL1) from cytosol to nucleus (*6*). In *Caenorhabditis elegans*, the pro-apoptotic molecule Egl-1 releases Ced-4 from mitochondria, which then travels to nuclear membranes (*7*). Site-specific cleavage of several hundred death substrates by dedicated proteases, called caspases, is a critical step in the execution phase of apoptosis (*8*). For example, cleavage of the chaperone ICAD releases its partner CAD (caspase-activated deoxyribonuclease), which translocates to the nucleus to degrade DNA (*9*, *10*). Other caspase substrates include DNA repair enzymes, structural components of the cytoskeleton or nuclear scaffold, and BCL-2 family proteins that affect mitochondrial dysfunction (*8*, *11–14*). This includes the pro-apoptotic molecule BID, a member of the "BH3 domain only" subset that links proximal signals from death receptors to the common apoptotic pathway (*11–13*). Engagement of the receptor Fas (CD95) or of tumor necrosis factor receptor 1 (TNFR1) activates caspase 8, which cleaves the inactive cytosolic form of BID (p22), generating a truncated 15-kd fragment (tBID) (*11–13*) that relocates to mitochondria within 1 hour. The exposed BH3 domain of tBID (*15*, *16*) binds and oligomerizes BAK, a resident mitochondrial family member with multiple BH domains, resulting in mitochondrial dysfunction, including the release of cytochrome c (*17*). How BID rapidly and selectively targets the mitochondrial outer membrane remains unresolved.

Multidimensional nuclear magnetic resonance analysis indicated that uncleaved and cleaved BID have approximately the same conformation in solution, suggesting that the p7 and p15 fragments remain in a noncovalent complex after cleavage by caspase 8 (*15*). Consequently, we explored the mechanism by which this complex translocated to and inserted into the mitochondrial membrane. We confirmed that the p15 tBID fragment was not released when recombinant full-length p22 was cleaved by caspase 8. When NH_2-terminal histidine-tagged p7 (his-p7) was released from a nickel agarose column by imidazole, the p15 tBID fragment always coeluted (Fig. 1A, lane 1), suggesting a tight noncovalent complex. The solution structure of p22 BID suggests that a hydrophobic interaction between α1 and α3 helices may be responsible (*15*, *16*). In support of this idea, p15 was only dissociated from his-p7 when the nonionic detergent *n*-octyl glucoside reached its critical micelle concentration (0.6% w/v), indicating a strong hydrophobic interaction (Fig. 1A) (*15*, *18*). We

Howard Hughes Medical Institute, Dana-Farber Cancer Institute, Departments of Pathology and Medicine, Harvard Medical School, Boston, MA 02115, USA.

*These authors contributed equally to this work.
†To whom correspondence should be addressed. E-mail: stanley_korsmeyer@dfci.harvard.edu

next compared the ability of intact p22, cleaved p7-p15 complex, and p15 tBID to target isolated mitochondria. The cleaved p7-p15 complex displayed little improvement in targeting over p22, whereas the isolated p15 fragment bound the mitochondrial membrane more efficiently (Fig. 1B). Treatment of the targeted mitochondria with alkali revealed that only the p15 appeared to be integral to the membrane, whereas any mitochondrial p22 was only loosely associated.

Despite the high stability and low targeting efficiency of the p7-p15 complex in vitro, tBID localizes to mitochondria very rapidly after cleavage in vivo (*13*). Thus, we searched for possible posttranslational modifications of BID that would promote its translocation and membrane insertion, as it lacks the typical hydrophobic COOH-terminus that serves as a signal/anchor sequence for other BCL-2 family members (*19*). Phosphorylation of BID does not appear to play a role, because neither Fas nor TNFR1 activation affected the phosphorylation of BID. Subsequently, we assessed BID for lipid modification and found that BID was not palmitoylated. However, we noted that an NH_2-terminal glycine would be generated upon cleavage by caspase 8 and that this conserved site on the p15 fragment (GSQASR) (*20*) conformed to a consensus myristoylation site (*3*). Although N-myristoylation of mammalian proteins has previously been described only as a cotranslational modification of nascent polypeptides (*3*), we tested whether BID could be myristoylated posttranslationally after cleavage by caspase 8. Jurkat cells were metabolically labeled with [^{3}H]myristic acid, then treated with an antibody (Ab) to Fas. Immunoprecipitation of proteins from cell extracts with an Ab to BID revealed that p15 BID, but not p22, was myristoylated (Fig. 2A). Furthermore, the linkage of myristic acid to p15 was resistant to treatment with 0.2 M KOH and 1 M hydroxylamine, indicating an amide linkage characteristic of myristoylation (Fig. 2A), which can occur at NH_2-terminal glycines or occasionally at internal lysine residues. We developed an in vitro myristoylation assay using rabbit reticulocyte lysate to map the site(s) of myristoylation in the p7-p15 complex. Substitution of Gly^{60} with Ala (G60A) abolished myristoylation of the p15 fragment completely, whereas mutation of internal lysine residues had no effect (Fig. 2, B and C). Caspase 8 cleaved recombinant G60A p22 as efficiently as it did wild-type (wt) p22 BID in vitro (Fig. 2D).

To study the functional significance of BID myristoylation, we tested whether N-myristoyltransferase (NMT), the enzyme responsible for cotranslational myristoylation (*3*), would also catalyze posttranslational myristoylation of BID. Recombinant NMT myristoylated the cleaved p7-p15 wt complex but not the G60A complex in vitro (Fig. 3A). Furthermore, myristoylation of the p7-p15 complex markedly enhanced targeting of myr-p15 to mitochondria. Whereas <30% of the p7-G60A p15 complex would associate with mitochondria, essentially 100% of p7-myr-p15 associated with the sedimented mitochondria (Fig. 3B). The myr-p15 proved alkaline-resistant (as above), which supports an integral membrane position. We next tested whether myristoylation might promote dissociation of the p7-p15 complex. A noncovalent complex of wt or G60A BID was myristoylated, and the interaction between his-p7 and p15 assessed by using nickel-agarose beads to capture p7. All of the [^{3}H]myristoylated p15 was associated with p7 (Fig. 3C), indicating that myristoylation did not in and of itself cause dissociation of the complex. Alternatively, myristoylation of the p7-p15 complex might improve targeting to selected membranes, in particular the outer mitochondrial membrane, with its unique lipid composition (*21*). The p7-p15 complex did not associate with standard liposomes in the absence of myristoylation, but the p7-myr-p15 complex did (Fig. 3D). This suggests that no specific protein target is absolutely re-

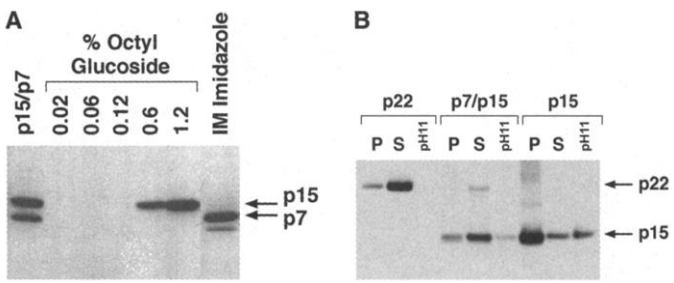

Fig. 1. Analysis of the noncovalent BID complex (p7-p15). (**A**) Dissociation of the p7-p15 complex with octyl glucoside (*26*). The histidine-tagged p22 BID was cleaved by recombinant caspase 8 (lane 1) and applied to a nickel-affinity column. p15 was eluted from the column-bound p7 with the indicated concentrations of octyl glucoside in the wash buffer. His-p7 was then eluted with 1 M imidazole. The fractions were analyzed by SDS-PAGE and stained with Coomassie blue. (**B**) In vitro targeting of recombinant p22, p7-p15 complex, or p15 BID to isolated liver mitochondria (*26*). The mitochondrial pellets (P) and the supernantant (S) were separated by centrifugation. Samples were also taken from mitochondrial pellets treated with an alkaline solution [0.1 M Na_2CO_3 (pH 11)]. The samples were size-fractionated by SDS-PAGE and analyzed by protein immunoblot analysis with an Ab to BID.

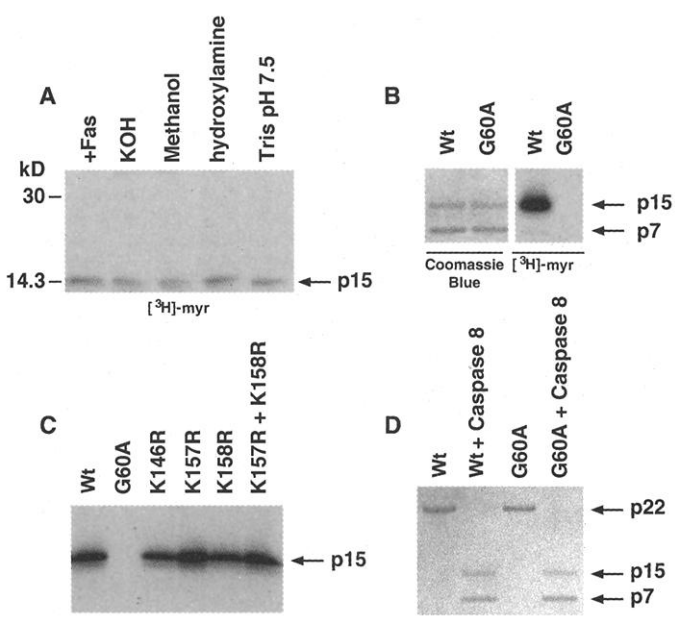

Fig. 2. Characterization of BID myristoylation and identification of the modification site. (**A**) Metabolic labeling of Jurkat cells with [^{3}H]myristic acid and analysis of fatty acid linkage to BID (*27*). Jurkat cells were labeled with [^{3}H]myristic acid overnight and subsequently activated with an Ab to Fas. Proteins from cellular lysates prepared 1 hour after activation were immunoprecipitated with an Ab to BID and fractionated by SDS-PAGE. Gel slices were treated with 0.2 M KOH, methanol, 1 M hydroxylamine (pH 7.5), or 1 M tris (pH 7.5), and autoradiograms were developed. (**B**) In vitro myristoylation of the p7-p15 complex. The wt or G60A p7-p15 complex was treated with rabbit reticulocyte lysate in the presence of 20 μCi [^{3}H]myristic acid at 30°C for 30 min. The samples were fractionated by SDS-PAGE, and an autoradiogram was developed. The input wt and G60A p7-p15 complexes were stained with Coomassie blue. (**C**) Mapping of the myristoylation site within BID (*20*). Site-directed mutagenesis was used to generate p15 BID mutants in which potential myristoylation sites were replaced. The p15 BID mutants were translated in vitro in the presence of 20 μl of [^{3}H]myristic acid, using rabbit reticulocyte lysate. The translated products were immunoprecipitated with an Ab to BID, separated by SDS-PAGE, and exposed for autoradiography. (**D**) Cleavage of wt and G60A p22 by recombinant caspase 8 (20:1, w/w) at 30°C for 1 hour. The full-length p22 and the cleavage products were separated by SDS-PAGE and stained with Coomassie blue.

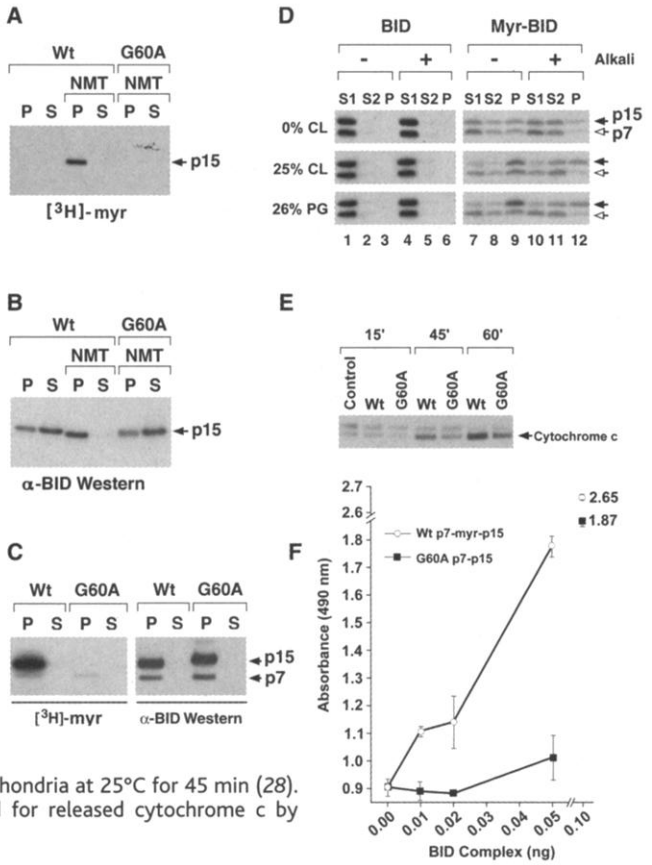

Fig. 3. Targeting of the myristoylated p7-p15 complex of BID to mitochondria and liposomes. (**A**) In vitro myristoylation of the p7-p15 complex by NMT. The wt or G60A p7-p15 complexes were treated with recombinant NMT (*28*) at 30°C for 30 min in the presence of 4.3 μM [^{3}H]myristoyl CoA and were subsequently used in an in vitro targeting assay with isolated mouse liver mitochondria. The mitochondrial pellet (P) and supernatant (S) were separated by SDS-PAGE, and an autoradiogram was developed. (**B**) Targeting of BID to mitochondria. The mitocondrial pellet and supernatant from the same experiment shown in (A) were analyzed by protein immunoblot analysis with an Ab to BID. (**C**) Myristoylation does not cause the dissociation of the p7-p15 complex (*28*). The histidine-tagged p7-p15 complex was myristoylated in vitro by NMT in the presence of [^{3}H]myristoyl CoA. His-p7 was sedimented with nickel agarose beads as the pellet (P) separated from the supernatant (S). Proteins were fractionated by SDS-PAGE, followed by exposure for autoradiography or protein immunoblotting. (**D**) Targeting of BID to liposomes (*28*). p7/myr-p15 (Myr-BID) and nonmyristoylated BID complexes were incubated with liposomes bearing the lipid composition of the mitochondrial outer membrane (0% CL) or of outer membrane contact sites, which include CL (25%) (*21*, *22*) or substitution of phosphatidylglycerol for CL to maintain negative charge (26% PG). The liposomes were pelleted and separated from the supernatant (S1) by ultracentrifugation, and then washed once more by either a neutral buffer [150 mM KCl and 20 mM Hepes (pH 7.0)] or an alkaline solution [0.1 M Na_2CO_3 (pH 11)] and ultracentrifuged again. Samples of the liposome pellet (P) and the second supernatant (S2) were fractionated by SDS-PAGE and stained with Coomassie blue. (**E**) Effect of myristoylation of BID-induced release of cytochrome c from mitochondria. The wt or G60A p7-p15 complex was treated with recombinant NMT in the presence of myristoyl CoA and was subsequently incubated with isolated mitochondria at 25°C for 15, 45, and 60 min (*28*). The supernatant was separated from the mitochondrial pellets and analyzed with an Ab to cytochrome c (Pharmingen). (**F**) Effect of myristoylation on dose response of BID-induced cytochrome c release from mitochondria. Increasing amounts of myristoylated wt or G60A p7-p15 complex (freshly prepared as above) were incubated with isolated mitochondria at 25°C for 45 min (*28*). The supernatant was separated from the mitochondrial pellets and analyzed for released cytochrome c by enzyme-linked immunosorbent asssay (Quantikine, R&D Systems).

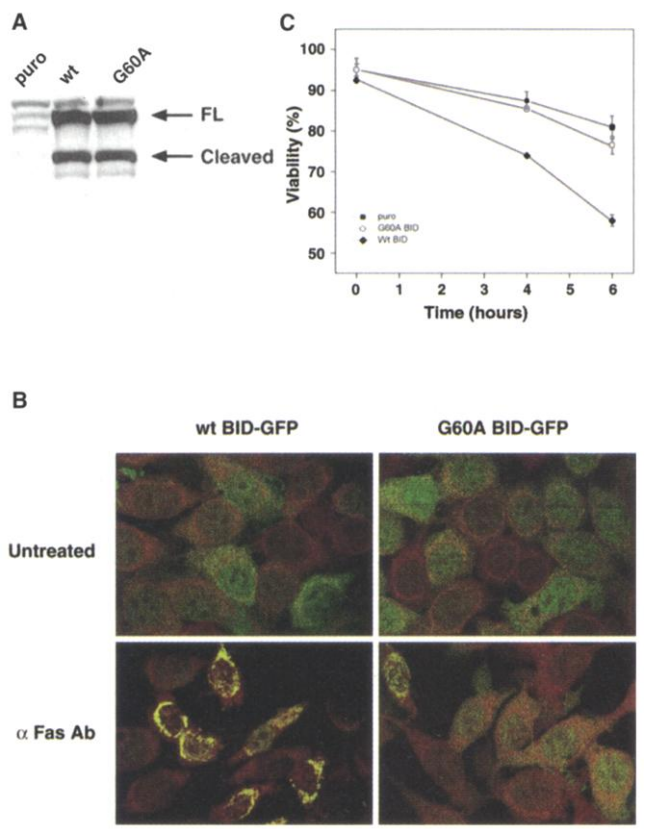

Fig. 4. Decreased translocation to mitochondria and reduced pro-apoptotic activity of the nonmyristoylatable mutant of BID. (**A**) Protein immunoblot analysis of BID in Fas-activated MCF7 cells. MCF7 cells expressing human Fas were infected with recombinant retrovirus possessing either full-length wt or G60A BID bearing a COOH-terminal GFP tag and a puromycin-resistance gene. The bulk population of puromycin-resistant MCF7 cells was treated with Ab to Fas and cyclohexmide for 4 hours, and total cell lysates were analyzed by protein immunoblotting with an Ab to BID. The positions of full-length BID-GFP (FL) and p15-GFP (cleaved) are indicated by arrows. (**B**) Subcellular localization of wt versus G60A BID. BID-GFP–expressing MCF7 cells were either treated with Ab to Fas and cycloheximide for 4 hours or left untreated. Mitochondria were identified with 150 nM Mitotracker, which was incubated with the cells for 30 min before fixation. The subcellular colocalization of BID-GFP (green fluorescence) and mitochondria (red fluorescence) was assessed by confocal microscopy. (**C**) Viability of the retrovirus-infected MCF7 cells after Fas activation. The MCF7 cells with wt BID, G60A BID, or the empty vector control (puro) were treated with an Ab to Fas and cycloheximide. At indicated time points, cells were stained with propidium iodide (PI, 1 μg/ml), and the percentage of the viable cells (PI-negative population) was determined by flow cytometry. Data reflect duplicate assays and are representative of two independent puromycin-selected populations of MCF7 cells expressing wt or G60A BID-GFP (*29*).

quired for targeting of myr-BID. Liposomes containing cardiolipin [to reflect the lipid composition determined for the outer mitochondrial membrane at contact sites (*21*), where tBID clusters] displayed a modestly increased binding of the myristoylated complex (Fig. 3D). However, liposomes in which phosphatidylglycerol was substituted for cardiolipin to maintain charge showed similar binding, suggesting that the overall net negative charge, rather than individual lipids, may account for the improvement (Fig. 3D). Alternatively, a study that targeted the nonmyristoylated form of p15 tBID to liposomes proposed that cardiolipin provides a unique structure to the membrane (*22*). Much of the myr-p15 used here proved resistant to dissociation under alkaline conditions, whereas associated p7 was released, consistent with the nonintegral location noted for p7 at mitochondria (*12*). Therefore, the improved targeting of p7-myr-p15 BID to mitochondria is achieved, at least in part, by a selective interaction between myr-p15 and the mitochondrial membrane. To determine whether the improved targeting of myr-p15 enhanced mitochondrial dysfunction, we assessed the release of cytochrome c. The p7-myr-p15 complex was also more efficient at releasing cytochrome c from isolated mitochondria than was a nonmyristoylated p7-G60A p15 complex in both a time course (Fig. 3E) and dose response (Fig. 3F) assessment. Release was initiated with 0.01 ng (9 fmol) of p7-myr-p15 complex per 1 mg of purified mitochondria. Similarly, 900 fmol of p7-myr-p15 BID will maximally release cytochrome c from 1 mg of mitochondria, whereas 320 pmol of nonmyristoylated p15 is required.

We next addressed the functional significance of BID myristoylation in subcellular trafficking and cell death in vivo. Either wt or G60A p22 BID, each bearing a COOH-terminal green fluorescent protein (GFP) tag, was stably expressed in a bulk population of MCF7 cells, which also expressed human Fas. A similar amount of p15-GFP fragment was generated from wt or G60A BID cells activated with Ab to Fas (Fig. 4A). Confocal microscopy revealed that most cells expressing wt BID-GFP displayed a redistribution of GFP after Fas activation from a diffuse cytosolic distribution to a clustered localization that was coincident with mitochondria, as assessed with Mitotracker stain (Fig. 4B). In contrast, most cells bearing G60A BID-GFP retained a diffuse cytosolic localization of GFP after Fas activation (Fig. 4B). Furthermore, only the additional wt BID-GFP, but not comparable amounts of the G60A mutant, accelerated apoptosis of MCF7 cells after Fas activation (Fig. 4C). Taken together, these data indicate that myristoylation of BID promotes its targeting to mitochondria as well as enhances its pro-apoptotic activity in vivo.

BID provides an example of an unexpected posttranslational N-myristoylation, resulting in a selective pathway of subcellular trafficking. Sixteen of ~60 identified caspase substrates expose an NH_2-terminal glycine upon cleavage (*8*), which, combined with the loose consensus motif for myristoylation, suggests that this paradigm could prove a common modification in apoptosis and perhaps other proteolytic pathways. Assessment of the p7-myr-p15 BID complex indicates that N-myristoylation has a strong influence on BID selecting mitochondria, inserting into the outer membrane, releasing cytochrome c, and killing cells. Specifically, the enhanced movement of myristoylated BID from cytosol to mitochondria in vivo is apparently compounded by improved insertion of myristoylated BID into membranes. Myristoylation has been associated with proteins in other membrane compartments and also been observed to modulate protein-protein or protein-lipid interactions. Cotranslational myristoylation of NADH (the reduced form of nicotinadimide adenine dinucleotide) cytochrome b5 reductase does appear to be required for its mitochondrial localization (*23*). Taken together, the myristic acid moiety itself is unlikely to be the selective targeting motif; instead, the N-myristoylation of the BID complex appears to promote a protein conformation that favors the mitochondrial outer membrane. Thus, the N-myristoylation of BID after proteolytic processing represents a molecular switch that helps ensure the next critical step in apoptosis: the release of cytochrome c and subsequent cell demise.

References and Notes

1. G. Blobel, *Cold Spring Harb Symp. Quant. Biol.* **60**, 1 (1995).
2. J. L. Goldstein, M. S. Brown, *Nature* **343**, 425 (1990).
3. D. R. Johnson, R. S. Bhatnagar, L. J. Knoll, J. I. Gordon, *Annu. Rev. Biochem.* **63**, 869 (1994).
4. T. Pawson, G. D. Gish, *Cell* **71**, 359 (1992).
5. J. Zha, H. Harada, E. Yang, J. Jockel, S. J. Korsmeyer, *Cell* **87**, 619 (1996).
6. A. Brunet *et al.*, *Cell* **96**, 857 (1999).
7. F. Chen *et al.*, *Science* **287**, 1485 (2000).
8. D. W. Nicholson, *Cell Death Differ.* **6**, 1028 (1999).
9. M. Enari *et al.*, *Nature* **391**, 43 (1998).
10. X. Liu, H. Zou, C. Slaughter, X. Wang, *Cell* **89**, 175 (1997).
11. H. Li, H. Zhu, C. J. Xu, J. Yuan, *Cell* **94**, 491 (1998).
12. X. Luo, I. Budihardjo, H. Zou, C. Slaughter, X. Wang, *Cell* **94**, 481 (1998).
13. A. Gross *et al.*, *J. Biol. Chem.* **274**, 1156 (1999).
14. E. H. Cheng *et al.*, *Science* **278**, 1966 (1997).
15. J. J. Chou, H. Li, G. S. Salvesen, J. Yuan, G. Wagner, *Cell* **96**, 615 (1999).
16. J. M. McDonnell, D. Fushman, C. L. Milliman, S. J. Korsmeyer, D. Cowburn, *Cell* **96**, 625 (1999).
17. M. C. Wei *et al.*, *Genes Dev.* **14**, 2060 (2000).
18. G. Kudla *et al.*, *J. Biol. Chem.* **275**, 22713 (2000).
19. M. Nguyen, D. G. Millar, V. W. Yong, S. J. Korsmeyer, G. C. Shore, *J. Biol. Chem.* **268**, 25265 (1993).
20. Single-letter abbreviations for the amino acid residues are as follows: A, Ala; G, Gly; K, Lys; Q, Gln; R, Arg; S, Ser.
21. D. Ardail *et al.*, *J. Biol. Chem.* **265**, 18797 (1990).
22. M. Lutter *et al.*, *Nature Cell Biol.* **2**, 754 (2000).
23. N. Borgese, D. Aggujaro, P. Carrera, G. Pietrini, M. Bassetti, *J. Cell. Biol.* **135**, 1501 (1996).
24. L. D. Mayer, M. J. Hope, P. R. Cullis, *Biochim. Biophys. Acta* **858**, 161 (1986).
25. D. S. Ory, B. A. Neugeboren, R. C. Mulligan, *Proc. Natl. Acad. Sci. U.S.A.* **93**, 11400 (1996).
26. The full-length murine *Bid* was cloned into pET15b and expressed in *Escherichia coli* BL21 (DE3). The protein was purified by nickel-affinity chromatography. Active recombinant caspase 8 was similarly expressed and purified. The recombinant BID protein (1 mg/ml) was incubated with caspase 8 at 100:1 (wt/wt) in 20 mM Pipes (pH 7.2), 100 mM NaCl, 10 mM dithiothreitol (DTT), 1 mM EDTA, 0.1% CHAPS, and 10% sucrose at room temperature (RT) for 18 hours. The cleaved p7-p15 complex was applied to a nickel-affinity column. p15 was eluted from the column-bound p7 with increasing concentrations of octyl glucoside. His-tagged p7 was eluted with 1 M imidazole. The mitochondria used for the in vitro targeting assay were isolated from mouse liver as described (*13*) and incubated with 15 ng of p22, p7-p15, or p15 at 30°C for 30 min in the buffer containing 70 nM adenosine triphosphate (ATP), 3.5 mM sodium succinate, 56 nM adenosine diphosphate, 1.4 mM K_2HPO_4, 175 mM sucrose, 17 mM Hepes, (pH 7.5), 80 mM KCl, 2 mM $MgCl_2$, and 1 μg of liver cytosolic protein. The mitochondrial pellet and supernatant were separated by centrifugation at 7000*g* for 10 min. The mitochondrial pellets were also treated with 0.1 M Na_2CO_3 on ice for 30 min and recentrifuged (at 170,000*g*). The samples were size-fractionated and analyzed by protein immunoblot analysis using an Ab to BID (13).
27. Jurkat cells (50×10^6) were metabolically labeled overnight with [^{3}H]myristic acid (200 μCi/ml) (NEN) in RPMI medium containing 5 mM sodium pyruvate and were treated with Ab CH11 to Fas (Upstate Biotechnology) at 100 ng/ml for 1 hour. The cell lysate was prepared in radioimmunoprecipitation buffer and was immunoprecipitated with an Ab to BID. The immunoprecipitate was size-fractionated by SDS–polyacrylamide gel electrophoresis (SDS-PAGE). Gel slices were treated with either 0.2 M KOH in methanol, methanol, 1 M hydroxlamine HCl (pH 7.5), or 1 M tris Cl (pH 7.5) for 1 hour at RT and were exposed for autoradiography. The in vitro transcription and translation system was obtained from Promega, and site-directed mutagenesis was performed with the Quikchange kit from Stratagene.
28. Murine *NMT-1* was cloned into the Eco RI site of pGEX3Z and expressed as a glutathione *S*-transferase fusion protein. The recombinant NMT-1 was purified with a glutathione affinity column. The p7-p15 BID complex was myristoylated in the buffer containing 20 mM tris (pH 7.5), 1 mM DTT, 5 mM $MgCl_2$, 5 mM ATP, and 4.3 μM [^{3}H]myristoyl coenzyme A (CoA) (ICN) in the presence or absence of NMT-1. The in vitro targeting assay was carried out as previously described. The in vitro pull-down assay was done with 20 μl of pre-swollen nickel agarose beads to capture 0.5 μg of previously myristoylated and histidine-tagged p7/p15 complex. Large unilamellar vesicles (LUVs) were prepared by freeze-thawing and rapid extrusion (*24*). The lipid composition was cholesterol (9% by weight), 1-palmitoyl-2-oleoyl-*sn*-glycero-3-phosphoethanolamine (22%), phosphatidylinositol (8%), and 1-palmitoyl-2-oleoyl-*sn*-glycero-phosphocholine (61%) (Avanti Polar Lipids Alabaster, AL). The weight of phosphocholine was correspondingly reduced in the liposomes containing 25% 1,1',2,2'-tetramyristoylcardiolipin (CL) or 26% 1-palmytoyl-2-deoyl-*sn*-3-[phospho-*rac* (1-glycerol)] (PG). The dried lipids (100 mg) were resuspended in 2 ml of 20 mM Hepes (pH 7.5) and 150 mM KCl, freeze-thawed five times, and rapidly extruded 20 times through two sheets of polycarbonate filters with 100-nm pores to produce LUVs. Protein (60 μg) and liposomes (1 mg) were mixed in 50 μl of buffer [150 mM KCl and 20 mM Hepes (pH 7.5)] for binding experiments for 1 hour at RT. For the cytochrome c release assays, 5 μM of wt or G60A p7-p15 complex was incubated with 20 μM myristoyl CoA and NMT at 30°C for 20 min in the myristoylation buffer described above. The complexes were then diluted with wheat germ extract and incubated for 15 min at 0°C. For the time course experiment, 0.2 ng of complex in 1 μl of wheat germ extract was incubated with isolated liver mitochon-

dria [50 μg of mitochondrial proteins in 50 μl of 250 mM sucrose, 10 mM Hepes, 1 mM ATP, 5 mM succinate, 0.08 mM ADP, 2 mM K_2HPO_4, 32 mM KCl, and 0.8 mM $MgCl_2$ (pH 7.4)] for the indicated times at 25°C. For the dose response experiment, indicated amounts of complex in 1 μl of wheat germ extract were incubated with isolated liver mitochondria [50 μg of mitochondrial proteins in 50 μl of 150 mM KC1, 10 mM tris, 1 mM K_2HPO_4, 5 mM glutamate, 2.5 mM malate, and 0.01 mM EGTA (pH 7.4)] for 45 min at 25°C.

29. Wt and G60A p22 BID with a COOH-terminal GFP fusion were cloned into the Bam HI and Eco RI sites of pBabe puro vector. The recombinant viruses were produced with a VSV-G packaging cell line (*25*). MCF7 cells were infected with the viruses and selected in Dulbecco's modified Eagle's medium containing puromycin (1.5 μg/ml). The puromycin-resistant cells were used for protein immunoblot analysis, viability, and confocal microscopy.

30. We thank R. C. Mulligan, E. S. Alnemri, V. M. Dixit, and R. J. Collier for providing the cell lines and reagents used in these experiments and E. D. Smith for assistance in preparing the manuscript. J.Z. is supported by a Howard Temin Award from the National Cancer Institute (K01 CA82231) and by NIH training grant T32 CA72320-01A1. Supported by NIH grant CA50239-13.

17 August 2000; accepted 26 October 2000

Requirement of the RNA Editing Deaminase ADAR1 Gene for Embryonic Erythropoiesis

Q. Wang, J. Khillan, P. Gadue, K. Nishikura*

The members of the ADAR (adenosine deaminase acting on RNA) gene family are involved in site-selective RNA editing that changes adenosine residues of target substrate RNAs to inosine. Analysis of staged chimeric mouse embryos with a high contribution from embryonic stem cells with a functional null allele for ADAR1 revealed a heterozygous embryonic-lethal phenotype. Most ADAR1$^{+/-}$ chimeric embryos died before embryonic day 14 with defects in the hematopoietic system. Our results suggest the importance of regulated levels of ADAR1 expression, which is critical for embryonic erythropoiesis in the liver.

The adenosine-to-inosine (A-to-I) RNA editing by ADAR (*1*) results in the creation of alternative splicing sites (*2*) or alteration of codons and, thus, leads to functional changes in proteins. Target genes for ADAR include ionotropic glutamate receptors (GluRs) (*3, 4*) and serotonin receptor 2C subtype (5-HT_{2C}R) (*5*) in the brain and hepatitis delta virus antigen (*6*) in the liver. Three separate ADAR gene family members (ADAR1 to ADAR3) that display substantial differences in their substrate and editing site selectivity (*7–13*) have been identified in humans and rodents. Both ADAR1 and ADAR2 are expressed in many tissues (*7–9, 13*), whereas ADAR3 is expressed only in the brain (*10, 14*). In view of the ubiquitous expression of ADAR1 and ADAR2, it has been predicted that A-to-I RNA editing is likely to extend to additional target genes yet to be identified (*15*).

Using a targeting vector construct in which the two exons, E12 and E13, corresponding to a part of the catalytic domain (*16*), were replaced with a PGK-neo gene, we created a mutation of the mouse ADAR1 gene in early passage (P13) R1 (*17*) embryonic stem (ES) cells (*18*). Four separate ADAR1$^{+/-}$ ES cell clones identified did not exhibit any obvious alteration in their morphology or growth. The level of functional ADAR1 mRNA (*19*) derived from the remaining ADAR1^{+} allele in the targeted ES cells was reduced to about half of that in ADAR1$^{+/+}$ R1 cells as expected (Fig. 1A). We attempted to prepare ADAR1 mutant mouse lines with the nonfunctional ADAR1^{-} gene locus by coaggregating the ES cell lines with blastocysts derived from FVB/N albino donor mice (*17*). However, we encountered difficulties in obtaining chimeric mice that could vertically transmit the ADAR1^{-} allele. The very limited number of mice that were born alive with a normal appearance were later found to be either nonchimeric or chimeras with a very limited contribution of ADAR1$^{+/-}$ cells (Table 1). These results led us to suspect embryonic lethality in ADAR1$^{+/-}$ chimeric mice. The double-stranded RNA (dsRNA) binding domains located from E2 to E7 (*16*) were not altered during targeting. Thus, a COOH-terminal–truncated ADAR1 protein without its deaminase domain, but capable of binding to substrate RNAs, could be generated from the ADAR1^{-} allele (*18*). Potentially such aberrant ADAR1 proteins, if translated, might compete with and thus inhibit the activity of the wild-type enzyme derived from the ADAR1^{+} allele (*10*). However, Western blot analysis with a specific monoclonal antibody (mAb) raised against the region E2 to E8, detected only wild-type ADAR1 proteins of the expected size in the ADAR1$^{+/-}$ ES cells at reduced level, 50 to 60% of that in ADAR1$^{+/+}$ R1 ES cells (Fig. 1B). This result makes it very unlikely that dominant-negative inhibition by a COOH-terminal–truncated ADAR1 protein is the mechanism for the observed heterozygous-lethal phenotype.

Embryonic teratomas derived from ADAR1$^{+/-}$ ES cells were next examined for potential deficiencies in their ability to differentiate. All tumors contained a variety of differentiated and undifferentiated tissues, but with an abundance of cells of neuronal origin (70 to ~90%). No obvious histological difference was found among tumors derived from ADAR1$^{+/+}$ (R1) or ADAR1$^{+/-}$ (cl 52 and cl 119) ES cells. Because these tumors were clonal in nature and thus homogeneous for ADAR1 alleles, total RNA was extracted and tested for several known A-to-I editing sites of GluR-B, GluR5, and GluR6 subunits and 5-HT_{2C}R RNA. In the ADAR1$^{+/-}$ tumors a significant decrease (20 to 40%) in editing efficiency was found at the R/G site of GluR-B, the Q/R site of GluR5, and the A and B sites of 5-HT_{2C}R RNA (Table 2). In vitro editing of these sites by ADAR1 has been previously demonstrated (*5, 7–12, 20*). In contrast, the editing efficiency of the Q/R site of GluR-B and the D site of 5-HT_{2C}R, previously shown to be edited in vitro by ADAR2, occurred at the same level in tumors derived from ADAR1$^{+/-}$ ES cells and R1 cells. Thus, inactivation of even a single copy of ADAR1 gene has significant effects on the overall A-to-I RNA editing efficiency of ADAR1 target genes. A similar decline in the extent of editing at several known sites has been reported also for ADAR2$^{+/-}$ heterozygote mice (*21*). These known sites, as well as currently unidentified ADAR1 target sites, are likely to be underedited in ADAR1$^{+/-}$ chimeric embryos (see below).

A series of experiments were next conducted in which the staged chimeric embryos were recovered at different time points, from embryonic day 9.5 (E9.5) to E18.5 (Table 1). Although ADAR1$^{+/-}$ chimeric embryos, at least up to stage E11.5, exhibited no obvious abnormality, no live chimeric embryo beyond E14.5 with a high degree of contribution by ADAR1$^{+/-}$ cells was recovered (Table 1). A small number of chimeric embryos, in which the contribution of ADAR1$^{+/-}$ cells was >90%, survived to E12.5 and E13.5 (Table 1). ADAR1 functional mRNA derived from the ADAR1^{+} allele, though at substantially reduced levels (40 to 50%), was detected in these surviving chimeric embryos (Fig. 1A). Thus, the heterozygous embryonic lethal phenotype of ADAR1$^{+/-}$ chimeric embryos appears not due to a gene imprinting mechanism. The tight dose-dependent, heterozy-

Wistar Institute, Philadelphia, PA 19104, USA.

*To whom correspondence should be addressed. E-mail: kazuko@wistar.upenn.edu